

NASA
TP
1213
c.1

NASA
Technical Paper 1213

AVRADCOM
Technical Report 78-24

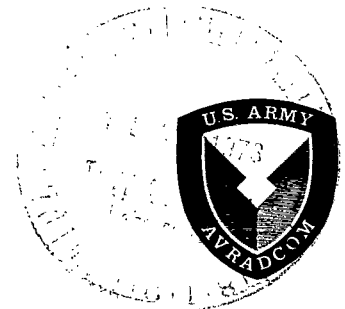
TECH LIBRARY KAFB, NM
0134569

LOAN COPY: RETURN TO
AFWL TECHNICAL LIBRARY
KIRTLAND AFB, NM

An Analysis of the Gust-Induced Overspeed Trends of Helicopter Rotors

Julian L. Jenkins, Jr., and William T. Yeager, Jr.

JULY 1978





NASA
Technical Paper 1213

AVRADCOM
Technical Report 78-24

An Analysis of the Gust-Induced Overspeed Trends of Helicopter Rotors

Julian L. Jenkins, Jr.
*Langley Research Center
Hampton, Virginia*

and

William T. Yeager, Jr.
*Structures Laboratory, AVRADCOM Research and Technology Laboratories
Langley Research Center
Hampton, Virginia*

NASA

National Aeronautics
and Space Administration

**Scientific and Technical
Information Office**

1978

SUMMARY

Equations for analyzing the potential gust-induced overspeed tendency of helicopter rotors are presented and discussed. A parametric analysis has also been carried out to illustrate the sensitivity of rotor angular acceleration to changes in rotor lift, propulsive force, tip speed, and forward velocity.

The results are in good agreement with a more complex and comprehensive nonlinear helicopter simulation analysis and indicate that an increase in helicopter gross weight increases the overspeed potential, whereas an increase in parasite drag decreases the overspeed potential.

INTRODUCTION

The gust response of helicopter rotors has been the subject of study for many years and, generally, a rotorcraft has been found to be less sensitive to gust-induced airloads than a fixed-wing aircraft (see, e.g., ref. 1). A recent incident, however, raised a question as to the sensitivity to gusts of the rotor rotational speed. For the incident considered, the rotorcraft reportedly encountered an intense gust which resulted in a rotor overspeed condition. Subsequent events led to other complications and, ultimately, a forced landing. The purpose of the analysis developed and presented herein is to characterize the initial gust-induced rotor overspeed tendency.

In order to examine the potential for a rotor overspeed and to assess the sensitivity of the problem, an analysis based on simple blade-element theory has been developed. The results of this parametric analysis and the equations used are presented in this paper. Correlation of the analysis with a more complex and comprehensive rotorcraft flight-simulation computer analysis is also presented.

SYMBOLS

The positive direction of forces, moments, and angles are depicted in figure 1.

a	rotor-blade-section mean lift-curve slope, 5.73/radian
a_1	longitudinal flapping coefficient of rotor tip-path plane, radians
$C_{D,R}$	rotor drag coefficient, $D_R/\rho\pi R^2(\Omega R)^2$
$C_{L,R}$	rotor lift coefficient, $L_R/\rho\pi R^2(\Omega R)^2$
$C_{P,i}$	rotor induced-power coefficient

$C_{P,O}$	rotor profile-power coefficient
$C_{P,P}$	rotor parasite-power coefficient
$C_{Q,E}$	engine torque coefficient, $Q/\rho\pi R^3(\Omega R)^2$
$C_{Q,R}$	rotor torque coefficient, $Q/\rho\pi R^3(\Omega R)^2$
C_{Ω}	rotor angular acceleration coefficient, $\dot{\Omega}I_P/\rho\pi R^3(\Omega R)^2$
D_R	rotor drag, newtons
f	helicopter equivalent flat-plate drag area, meter ²
I_P	rotor polar moment of inertia, kilograms-meter ²
L_R	rotor lift, newtons
Q	torque, newton-meters
R	rotor-blade radius, meters
v	rotor mean induced velocity, meters/second
V	airspeed, meters/second or knots
V_g	gust velocity, meters/second, positive upward
α	angle of attack of rotor control axis, radians
α_{TPP}	angle of attack of rotor tip-path plane, radians
δ	rotor-blade-section mean drag coefficient, 0.01
θ	rotor-blade collective pitch at 0.75R, radians
λ	inflow ratio, $(V \sin \alpha - v)/\Omega R$
μ	tip-speed ratio, $\approx V/\Omega R$
ρ	mass density of air, kilograms/meter ³
σ	rotor solidity; ratio of total blade area to disk area
Ω	rotor angular velocity, radians/second
$\dot{\Omega}$	rotor angular acceleration, radians/second ²

METHOD OF ANALYSIS

The analysis carried out herein is based on a development and solution of the torque balance equations for the rotor and uses the sign convention shown in figure 1. The equations are derived and presented in the appendix. The basic rotor acceleration equation given in terms of the defined acceleration coefficient is

$$C_{\dot{\Omega}} = - \left(C_{Q,E} + C_{Q,R} + \frac{\partial C_{Q,R}}{\partial \alpha} \frac{V_g}{V} \right) \quad (1)$$

It is apparent that the rotor can accelerate or overspeed only when the net value within the parentheses of equation (1) is negative (i.e., when the rotorcraft enters autorotative flight, or when the engine shaft torque supplied exceeds the rotor torque required, or when the gust perturbation is large and negative in sign). The solution to equation (1) involves solving for the initial rotor torque required $C_{Q,R}$ for the appropriate flight state, computation of the torque derivative $\frac{\partial C_{Q,R}}{\partial \alpha}$, and developing and solving an expression

for changes in the governor-controlled engine shaft torque supplied $C_{Q,E}$. For the parametric analysis conducted to obtain the trends predicted herein, the assumption was made that the shaft torque supplied remained constant at a value which equaled the initial torque required; that is, the fuel control governor system characteristics allowed the engine to accelerate the rotor when a gust disturbance reduced the rotor torque required. This approach has the advantages of being simpler to implement and is representative of the actual initial response of most governing systems. By using this approach, the rotor acceleration potential can be simply expressed as a function of the torque derivative and the disturbance gust as

$$C_{\dot{\Omega}} = - \frac{\partial C_{Q,R}}{\partial \alpha} \frac{V_g}{V} \quad (2)$$

where

$$\frac{\partial C_{Q,R}}{\partial \alpha} = \left(\frac{C_{L,R}}{\mu} - \mu \frac{C_{D,R}}{C_{L,R}} \right) \frac{\partial C_{L,R}}{\partial \alpha} - \mu C_{L,R} \left(1 + \frac{\partial a_1}{\partial \alpha} \right) \quad (3)$$

The solution of equation (2), as developed in the appendix, evolves from the expression for rotor torque based on the sum of profile power, induced power, and parasite power. This summation is

$$C_{Q,R} = \frac{\sigma\delta}{8} (1 + 3\mu^2) + \frac{(C_{L,R})^2}{2\mu} - C_{D,R}\mu \quad (4)$$

(See appendix, eq. (A8).) With the assumption made herein that the blade-section mean drag coefficient δ is constant, then the torque change due to a gust is basically dependent on changes in $C_{L,R}$ and $C_{D,R}$, which are associated with the rotor induced and parasite power terms of equation (4). As illustrated in figure 2, these changes are related through the angle α_{TPP} and its changes. The force diagram of figure 2(a) represents a trimmed flight condition. The force diagram of figure 2(b) represents changes which may occur when the trim is disturbed by the gust velocity V_g . The resultant torque change is thus dependent on the relative magnitude and sign of the changes in rotor lift and drag. The results of parametric variations in initial trim lift and drag for ranges of rotor speed and airspeed are presented in the following section. The calculations are not independent of rotor solidity even though the resultant acceleration coefficient is normalized by solidity.

RESULTS AND DISCUSSION

The analysis developed and presented in the appendix has been used to predict potential rotor overspeed tendencies for a range of initial rotor trim conditions. As discussed previously, the calculations were based on a constant value for engine shaft torque supplied. A sharp-edge, upward vertical gust of 9.144 m/sec was used as the disturbance velocity V_g . Thus, the magnitude of the rotor overspeed potential predicted by the analysis is determined by two factors: First, the rotor torque sensitivity to changes in angle of attack $\frac{\partial C_{Q,R}}{\partial \alpha}$; and second, the change in rotor angle of attack due to the gust $\Delta \alpha \approx V_g/V$. As previously indicated, the product $\frac{\partial C_{Q,R}}{\partial \alpha} \frac{V_g}{V}$ must be negative for a rotor overspeed potential to exist. Results from this analysis are presented in figure 3 for a realistic range of the parameters $C_{L,R}/\sigma$ and $f/\pi R^2$ at several values of rotor tip speed ΩR and airspeed V . For the calculations herein, the following characteristics were also assumed:

$$\sigma = 0.055$$

$$a = 5.73$$

$$\delta = 0.01$$

Overspeed Trends

Figure 3 has been assembled so that the parametric trends are readily assessed. For example, trends of the overspeed curves with increasing $C_{L,R}/\sigma$ at constant $f/\pi R^2$ are observed from top to bottom of each column of the figure, whereas trends of the overspeed with increasing $f/\pi R^2$ at constant

$C_{L,R}/\sigma$ are seen in the rows from left to right. Also, within the individual plots the effect of changes in airspeed and/or rotor rotational speed are shown. These trends are reviewed in subsequent paragraphs.

Effect of Gross Weight

A comparison of the columned plots of figure 3 (e.g., figs. 3(a), 3(d), 3(g), and 3(j)) shows that, for a given helicopter with fixed flat-plate drag f , an increase in gross weight, as reflected by $C_{L,R}/\sigma$, increases the maximum rotor overspeed potential due to the gust. The airspeed at which the maximum overspeed potential occurs also increases with $C_{L,R}/\sigma$. An assessment of equation (3), in consideration of these trends, indicates that the dominant factor is $C_{L,R}$. The first term $C_{L,R}/\mu$ arises from the induced-power term of equation (4) and, consequently, increases in gross weight are reflected in an increase in the induced-power contribution to the torque derivative. For an overspeed to occur under the conditions cited, the torque derivative must be negative in sign and the induced term must not have a negative value. Thus, for conditions shown in figure 3, where an overspeed potential is predicted, the predominant term is the third term in equation (3), that is, $\mu C_{L,R} \left(1 + \frac{\partial a_1}{\partial \alpha} \right)$, which arises from the parasite-power term of equation (4).

Effect of Flat-Plate Drag

The row plots of figure 3 (e.g., figs. 3(a), 3(b), and 3(c)) illustrate that for a helicopter with constant gross weight, an increase in flat-plate drag area $f/\pi R^2$ decreases the maximum overspeed potential at any given airspeed. This decrease results from the second term of equation (3) which, by combining

with $\frac{C_{D,R}}{\sigma} = - \frac{f}{\pi R^2} \frac{\mu^2}{2\sigma}$ (see appendix, eq. (A10)), can be shown to be propor-

tional to $f\mu^3$ and positive in sign. Thus, increases in the trim flat-plate drag decrease the overspeed tendency. Equally important to the overspeed trend is the tip-speed-ratio term μ^3 , which causes large changes with speed. In particular, at low-lift and high-drag conditions, as shown in figure 3(c), the increase in magnitude of the second term of equation (3) with speed is predominant in controlling the overspeed trend. However, at the high-lift and low-drag conditions illustrated in figure 3(j), the importance of the second term is diminished and the overspeed trends are again dominated by the third term

$\mu C_{L,R} \left(1 + \frac{\partial a_1}{\partial \alpha} \right)$ of equation (3). In any case, however, the airspeed at which the maximum overspeed potential occurs is inversely affected by the flat-plate drag.

Airspeed for Maximum Potential Overspeed

As previously mentioned, the airspeed at which the maximum rotor overspeed potential exists varies directly with the helicopter gross weight and inversely

with the flat-plate drag. For the range of conditions covered in figure 3, the curves show that the maximum overspeed potential occurs anywhere from 55 knots at the lowest gross weight and flat-plate drag condition of figure 3(a) to slightly over 140 knots at the highest gross weight and lowest drag condition of figure 3(j). This wide range in speed, however, is dictated by the relatively large range of lift-drag conditions evaluated, and the more representative conditions are those typified by the midrange values (i.e., figs. 3(e) and 3(h)). For these conditions, the airspeed for maximum rotor overspeed potential occurs between 60 and 100 knots. This speed range is of particular significance because a number of military helicopter operation manuals specify a gusty or turbulent air penetration velocity of 80 knots. This limit is dictated by other considerations, but for those helicopters which are susceptible to rotor overspeed and, in particular, those with low rotor polar moment of inertia and sluggish governor response characteristics, the rotor-speed fluctuation may be disconcerting.

To illustrate the significance of the overspeed parameter, consider the configuration

$$C_{L,R}/\sigma = 0.08$$

$$f/\pi R^2 = 0.009$$

$$V = 80 \text{ knots}$$

$$\Omega R = 198.12 \text{ m/sec}$$

$$R = 4.01 \text{ m}$$

$$\sigma = 0.055$$

$$I_p = 338.86 \text{ kg-m}^2$$

From figure 3(h), $C_{\dot{\Omega}}/\sigma = 2.25 \times 10^{-3}$ and therefore

$$\dot{\Omega} = \frac{C_{\dot{\Omega}}}{\sigma} \frac{\rho \pi R^2 (\Omega R)^2 R \sigma}{I_p} = 3.56 \text{ rad/sec}^2$$

Since the initial rotational speed is 49.39 rad/sec, the predicted overspeed tendency represents a potential 7.2-percent increase in rotor angular velocity for each second the acceleration persists.

Comparison of Simple Theory With Nonlinear Helicopter Theory

In order to validate the trends established by using the simple analysis developed herein, a comparison has been made between these simple blade-element-theory results and results obtained from a nonlinear helicopter simulation analysis described in reference 2. The nonlinear results were obtained by using the maneuver option of the program and allowing the simulated vehicle to encounter a 9.144-m/sec, sharp-edge, upward vertical gust. In order to simulate sluggish governor response characteristics, the value of the engine torque supplied to the main rotor was fixed throughout the maneuver at the value calculated as that torque required for the initial trimmed level flight. The rotor angular acceleration was determined from changes in the rotor rotational speed between the time the rotor first encountered the gust and the time at which the rotor had penetrated the gust a distance of two rotor diameters. This penetration interval provided a common basis for the calculation of $C_{\dot{\Omega}}$ by establishing a point in the maneuver where the rate of change of rotor rotational speed had essentially stabilized.

Two comparisons are made. Figure 4 shows a comparison of the simple results with the nonlinear predictions using steady, two-dimensional blade-section aerodynamic characteristics in the rotor analysis. The overspeed trends predicted by both methods are generally similar, although the nonlinear analysis indicates a more dramatic reduction in overspeed potential at the higher air-speeds. Because the nonlinear analysis accounts for the effects of rotor blade stall and compressibility and the present analysis does not, the torque derivative of the nonlinear analysis is probably more susceptible to increases in torque due to stall and thus does not show the same tendency to overspeed at high forward speeds.

As previously mentioned, the nonlinear analysis uses steady aerodynamics in computing rotor performance, and thus the rotor derivatives may be affected by the stall characteristics. In order to assess this effect, the nonlinear analysis was rerun by using an unsteady aerodynamics option (identified as BUNS in ref. 2). This unsteady option, which is probably a more realistic representation of transient rotor aerodynamics, results in a delay in blade-section lift stall and a retardation of section drag increase. The results of the nonlinear analysis with the unsteady option are also shown in figure 4. Inclusion of the unsteady aerodynamics effects generally results in better overall correlation with the linear analysis. This is perhaps not too surprising because the unsteady aerodynamic method used in reference 2 tends to maintain a more constant lift-curve slope and to produce less drag growth as rotor-blade-section angle is increased. Both characteristics are inherent in simple blade-element theory, and therefore the present analysis provides a very reasonable trending of the overspeed tendency of a helicopter rotor.

CONCLUSIONS

The simple analysis of the gust-induced overspeed trends of helicopter rotors reported herein has identified the basic parameters affecting rotor

overspeed and has provided a range of trending curves to illustrate the more important parameters. Specifically, analysis of the results leads to the following conclusions:

1. An increase in helicopter gross weight increases the overspeed potential.

2. An increase in helicopter parasite drag decreases the overspeed potential.

3. The airspeed at which the maximum overspeed potential occurs varies directly with gross weight and inversely with flat-plate drag area.

4. For representative values of helicopter lift and drag characteristics, the maximum overspeed potential occurs in the 60- to 100-knot airspeed range, which brackets the generally recommended 80-knot gust penetration airspeed limit.

5. The correlation of the simple analysis with a more complex and costly nonlinear helicopter simulation analysis, which included an unsteady aerodynamics routine, indicated that the simple analysis trends are very representative.

Langley Research Center
National Aeronautics and Space Administration
Hampton, VA 23665
May 24, 1978

APPENDIX

DEVELOPMENT OF EQUATIONS FOR ROTOR-OVERSPEED ANALYSIS

The basic equation necessary to determine the overspeed potential of a rotor system is based on the dynamical equation of the rotor shaft torque balance $\Sigma Q + I_p \dot{\Omega} = 0$ expressed as

$$\dot{\Omega} = - \frac{\rho \pi R^3 (\Omega R)^2}{I_p} \left(C_{Q,E} + C_{Q,R} + \frac{\partial C_{Q,R}}{\partial \alpha} \frac{V_g}{V} \right) \quad (A1)$$

where $C_{Q,R}$ is the initial trimmed value of rotor torque required. An acceleration coefficient is defined as

$$C_{\dot{\Omega}} \equiv \frac{\dot{\Omega} I_p}{\rho \pi R^3 (\Omega R)^2} \quad (A2)$$

Equation (A1) may then be written as

$$C_{\dot{\Omega}} = - \left(C_{Q,E} + C_{Q,R} + \frac{\partial C_{Q,R}}{\partial \alpha} \frac{V_g}{V} \right) \quad (A3)$$

The development of the equations necessary for solving equation (A3) are based on the simple blade-element theory as set forth in reference 3.

Rotor Torque Coefficient

Because the rotor shaft torque coefficient and the shaft power coefficient are equivalent, the expression for the rotor torque coefficient may be written as

$$C_{Q,R} = C_{P,O} + C_{P,i} + C_{P,p} \quad (\text{ref. 4}) \quad (A4)$$

APPENDIX

where, by integration, equation (26) of reference 5 may be expressed as

$$C_{P,O} = \frac{\sigma\delta}{8} (1 + 3\mu^2) \quad (A5)$$

With the assumption that the rotor thrust coefficient and rotor lift coefficient $C_{L,R}$ are equivalent and that $[1 + (\lambda/\mu)^2]^{1/2} \approx 1$, equation (7) of reference 4 may be expressed as

$$C_{P,i} \approx \frac{C_{L,R}^2}{2\mu} \quad (A6)$$

and with the additional assumption that $\cos \alpha \approx 1$, equation (8) of reference 4, may be expressed as

$$C_{P,p} \approx \frac{f}{\pi R^2} \frac{\mu^3}{2} = -C_{D,R}\mu \quad (A7)$$

Substitution of equations (A5), (A6), and (A7) into equation (A4) yields

$$C_{Q,R} = \frac{\sigma\delta}{8} (1 + 3\mu^2) + \frac{C_{L,R}^2}{2\mu} - C_{D,R}\mu \quad (A8)$$

or

$$\frac{C_{Q,R}}{\sigma} = \frac{\delta}{8} (1 + 3\mu^2) + \left(\frac{C_{L,R}}{\sigma} \right)^2 \frac{\sigma}{2\mu} - \frac{C_{D,R}}{\sigma} \mu \quad (A9)$$

By expressing $C_{D,R}/\sigma$ as

$$\frac{C_{D,R}}{\sigma} = - \frac{f}{\pi R^2} \frac{\mu^2}{2\sigma} \quad (A10)$$

APPENDIX

equation (A9) becomes

$$\frac{C_{Q,R}}{\sigma} = \frac{\delta}{8}(1 + 3\mu^2) + \left(\frac{C_{L,R}}{\sigma}\right)^2 \frac{\sigma}{2\mu} + \frac{f}{\pi R^2} \frac{\mu^3}{2\sigma} \quad (A11)$$

Rotor Torque Derivative

The rotor torque derivative is obtained by a partial differentiation of equation (A8) with respect to rotor angle of attack. The resulting expression is

$$\frac{\partial C_{Q,R}}{\partial \alpha} = \frac{C_{L,R}}{\mu} \frac{\partial C_{L,R}}{\partial \alpha} - \mu \frac{\partial C_{D,R}}{\partial \alpha} \quad (A12)$$

With the assumption that the resultant force vector is perpendicular to the rotor tip-path plane (see fig. 2), then

$$C_{D,R} \approx C_{L,R} \alpha_{TPP} \quad \text{or} \quad \alpha_{TPP} \approx \frac{C_{D,R}}{C_{L,R}} \quad (A13)$$

Thus,

$$\frac{\partial C_{D,R}}{\partial \alpha} = \frac{\partial C_{L,R}}{\partial \alpha} \alpha_{TPP} + C_{L,R} \frac{\partial \alpha_{TPP}}{\partial \alpha} \quad (A14)$$

Since, from figure 1

$$\alpha_{TPP} = \alpha + a_1 \quad (A15)$$

then

$$\frac{\partial \alpha_{TPP}}{\partial \alpha} = 1 + \frac{\partial a_1}{\partial \alpha} \quad (A16)$$

APPENDIX

Equations (A12), (A13), (A14), and (A16) can be combined to give

$$\frac{\partial C_{Q,R}}{\partial \alpha} = \left(\frac{C_{L,R}}{\mu} - \mu \frac{C_{D,R}}{C_{L,R}} \right) \frac{\partial C_{L,R}}{\partial \alpha} - \mu C_{L,R} \left(1 + \frac{\partial a_1}{\partial \alpha} \right) \quad (A17)$$

Rotor Lift Derivative

The rotor lift derivative may be obtained from

$$C_{L,R} = \frac{\sigma a}{4} \left[\theta \left(\frac{2}{3} + \mu^2 \right) + \lambda \right] \quad (\text{ref. 3}) \quad (A18)$$

and

$$\lambda = \frac{V \sin \alpha}{\Omega R} - \frac{v}{\Omega R} = \frac{V \sin \alpha}{\Omega R} - \frac{C_{L,R}}{2\mu \left(1 + \frac{\lambda^2}{\mu^2} \right)^{1/2}} \quad (A19)$$

or

$$\lambda = \mu \alpha - \frac{C_{L,R}}{2\mu} \quad (A20)$$

By substituting equation (A20) into equation (A18) to solve for $C_{L,R}$ and by taking the partial derivative with respect to α , the lift derivative may be expressed as

$$\frac{\partial C_{L,R}}{\partial \alpha} = \frac{2\mu^2}{1 + \frac{8\mu}{\sigma a}} \quad (A21)$$

APPENDIX

Rotor Flapping Derivative

The rotor flapping derivative may be obtained from

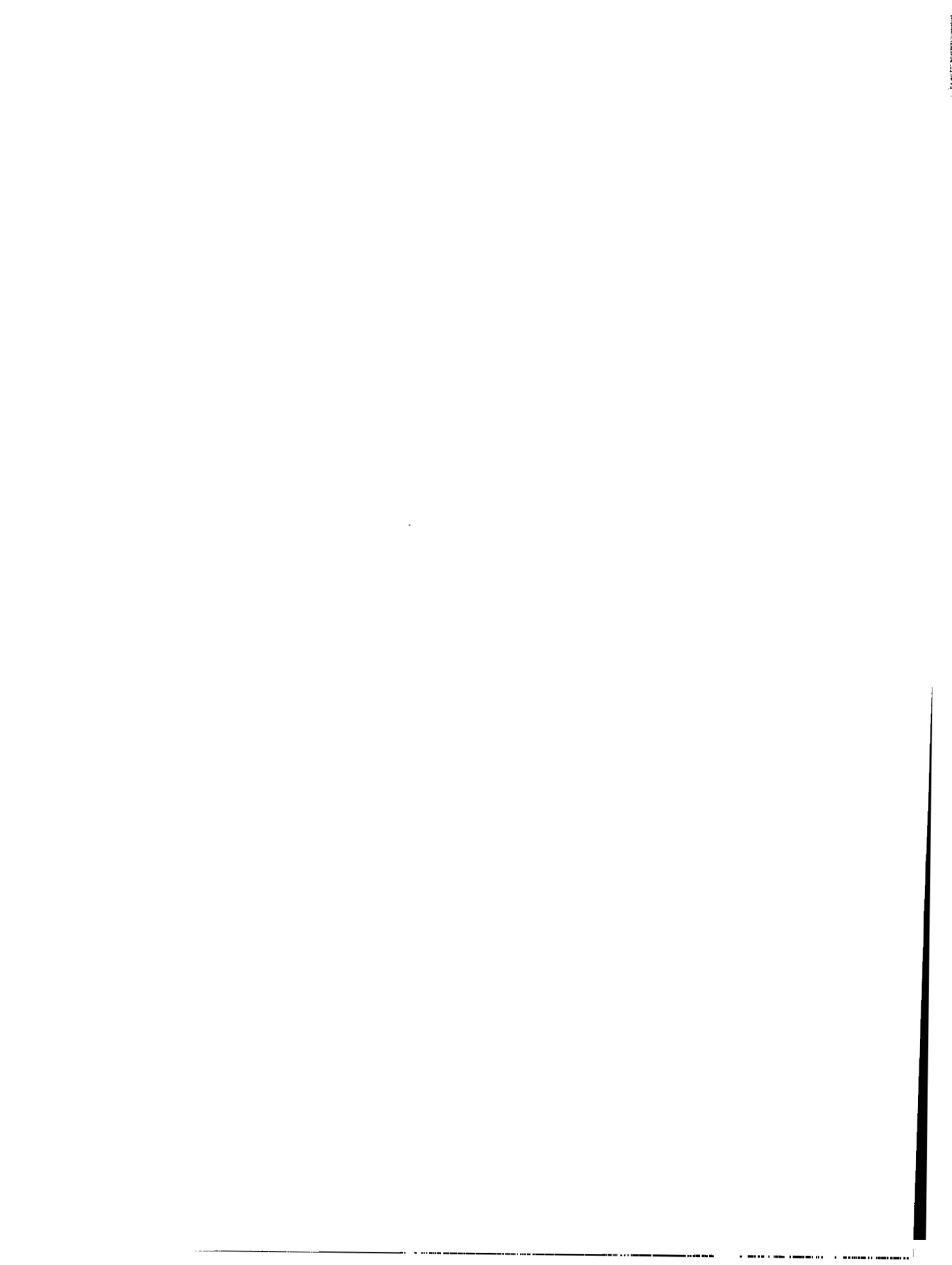
$$a_1 = \left(\frac{2\mu}{1 - \frac{1}{2}\mu^2} \right) \left(\frac{4}{3}\theta + \lambda \right) \quad (\text{ref. 3}) \quad (\text{A22})$$

Combining equations (A20) and (A22) and differentiating and substituting equation (A21) yields

$$\frac{\partial a_1}{\partial \alpha} = \left(\frac{4\mu^2}{2 - \mu^2} \right) \left(\frac{1}{1 + \frac{\sigma a}{8\mu}} \right) \quad (\text{A23})$$

Overspeed Solution

Equations (A11), (A17), (A21), and (A23) are used in the solution of equation (A3) for the overspeed coefficient. The computation requirements are minimal and can be carried out on a programmable pocket calculator. For the computations of this paper the engine shaft torque was assumed to be a constant value equal in magnitude but of opposite sign to the initial rotor torque required.



REFERENCES

1. Crim, Almer D.: Gust Experience of a Helicopter and an Airplane in Formation Flight. NACA TN 3354, 1954.
2. McLarty, Tyce T.: Rotorcraft Flight Simulation With Coupled Rotor Aeroelastic Stability Analysis. Volume I - Engineer's Manual. USAAMRDL-TR-76-41A, U.S. Army, May 1977. (Available from DDC as AD A042 462.)
3. Gessow, Alfred; and Myers, Garry C., Jr.: Aerodynamics of the Helicopter. Macmillan Co., c.1952.
4. Gessow, Alfred; and Tapscott, Robert J.: Charts for Estimating Performance of High-Performance Helicopters. NACA Rep. 1266, 1956. (Supersedes NACA TN 3323 by Gessow and Tapscott and TN 3482 by Tapscott and Gessow.)
5. Gessow, Alfred: Equations and Procedures for Numerically Calculating the Aerodynamic Characteristics of Lifting Rotors. NACA TN 3747, 1956.

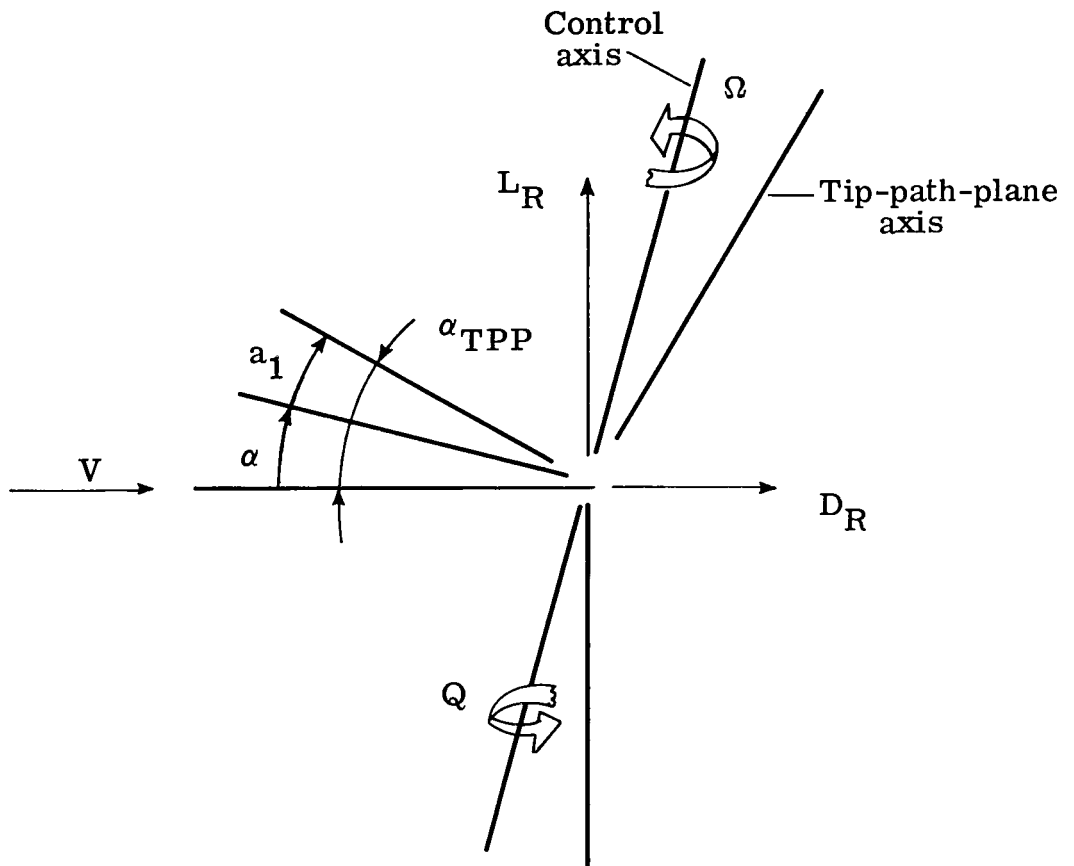
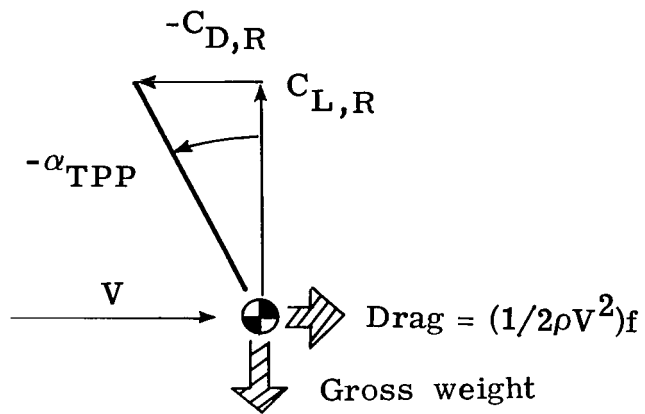
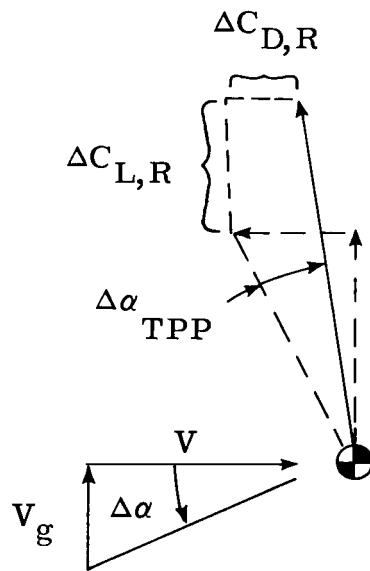


Figure 1.- Notation showing positive direction of forces and angles.



(a) Trimmed force diagram.



(b) Disturbed force diagram.

Figure 2.- Graphical representation of trimmed and disturbed rotor force components.

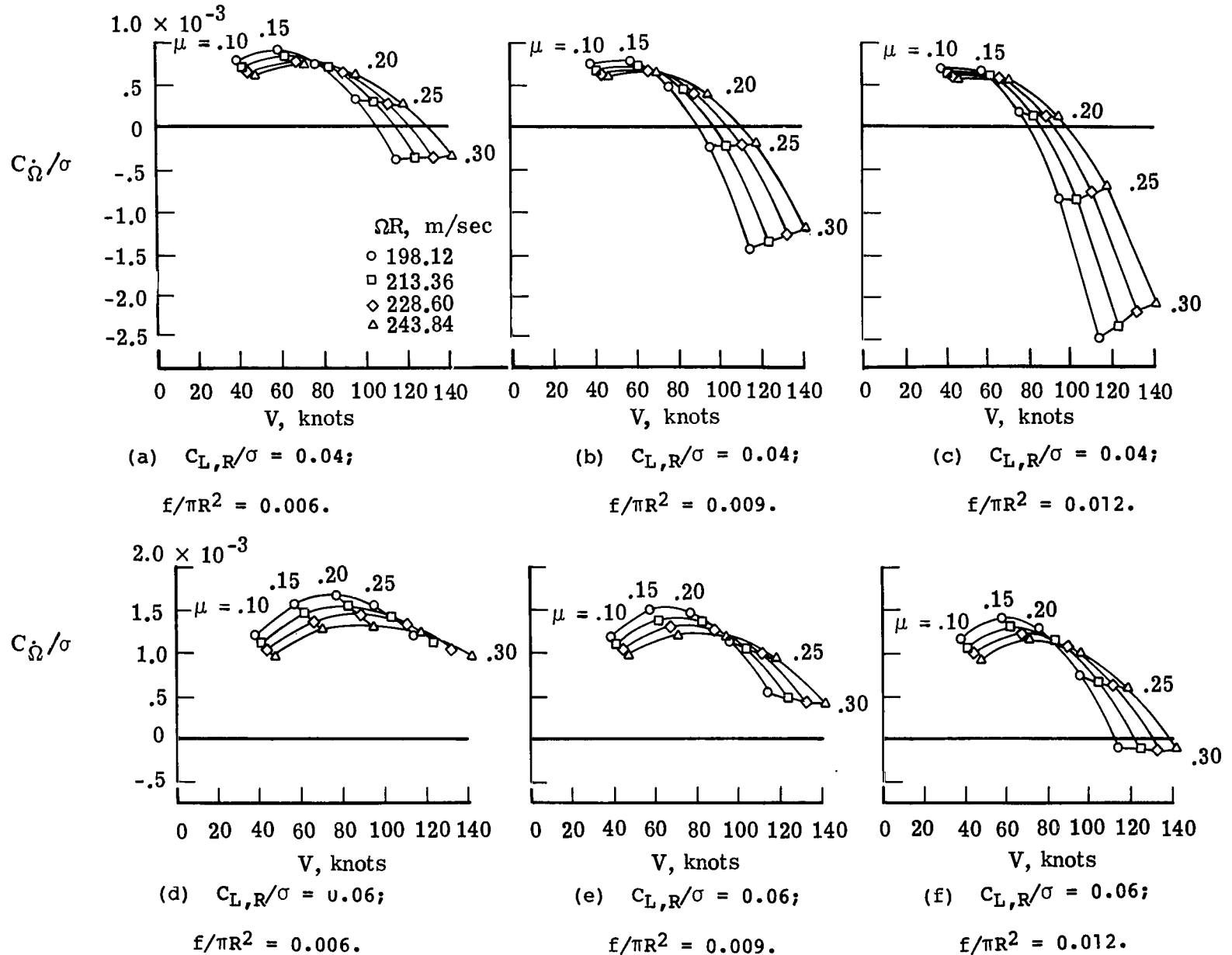
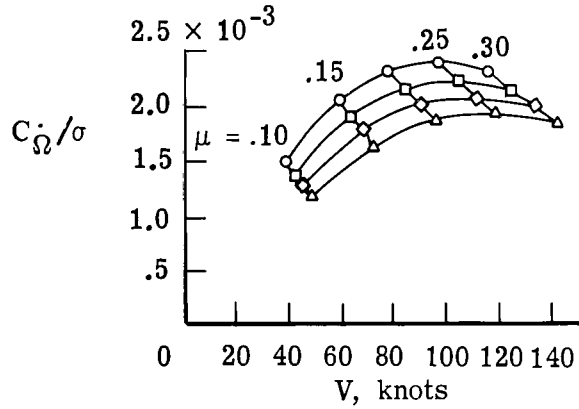
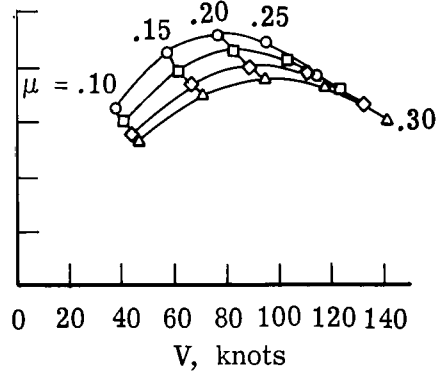


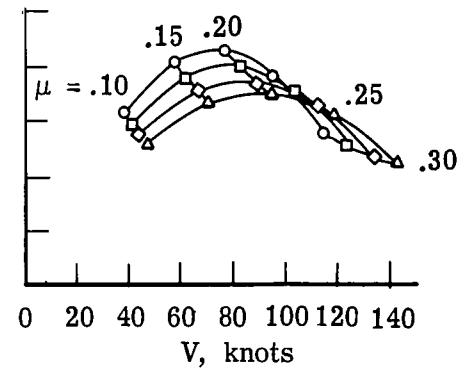
Figure 3.- Predicted rotor overspeed potential for a rotor with solidity equal to 0.055.



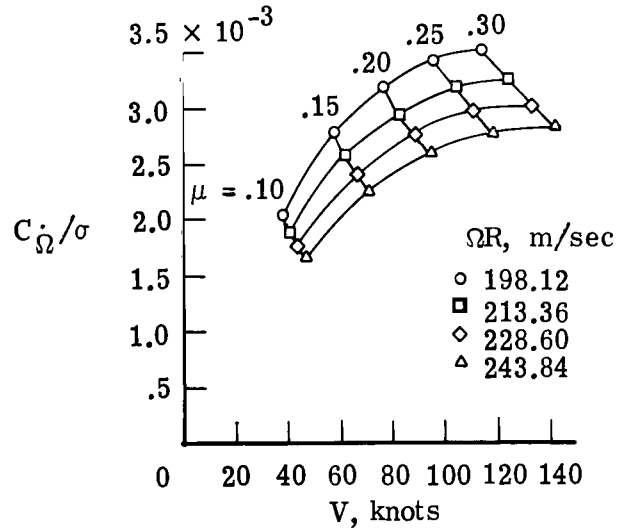
(g) $C_{L,R}/\sigma = 0.08$;
 $f/\pi R^2 = 0.006$.



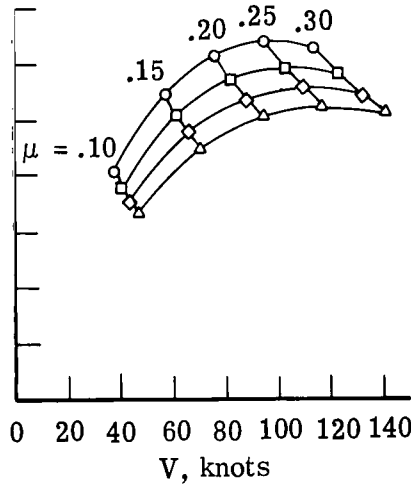
(h) $C_{L,R}/\sigma = 0.08$;
 $f/\pi R^2 = 0.009$.



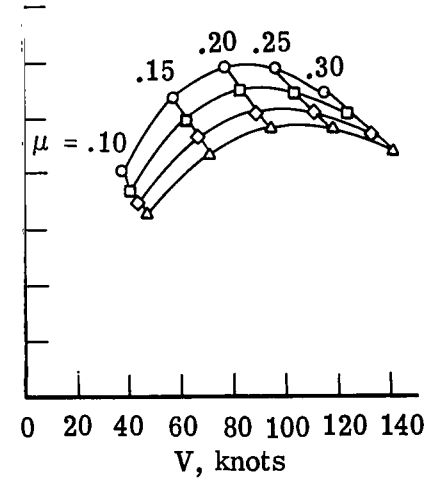
(i) $C_{L,R}/\sigma = 0.08$;
 $f/\pi R^2 = 0.012$.



(j) $C_{L,R}/\sigma = 0.10$;
 $f/\pi R^2 = 0.006$.



(k) $C_{L,R}/\sigma = 0.10$;
 $f/\pi R^2 = 0.009$.



(l) $C_{L,R}/\sigma = 0.10$;
 $f/\pi R^2 = 0.012$.

Figure 3.- Concluded.

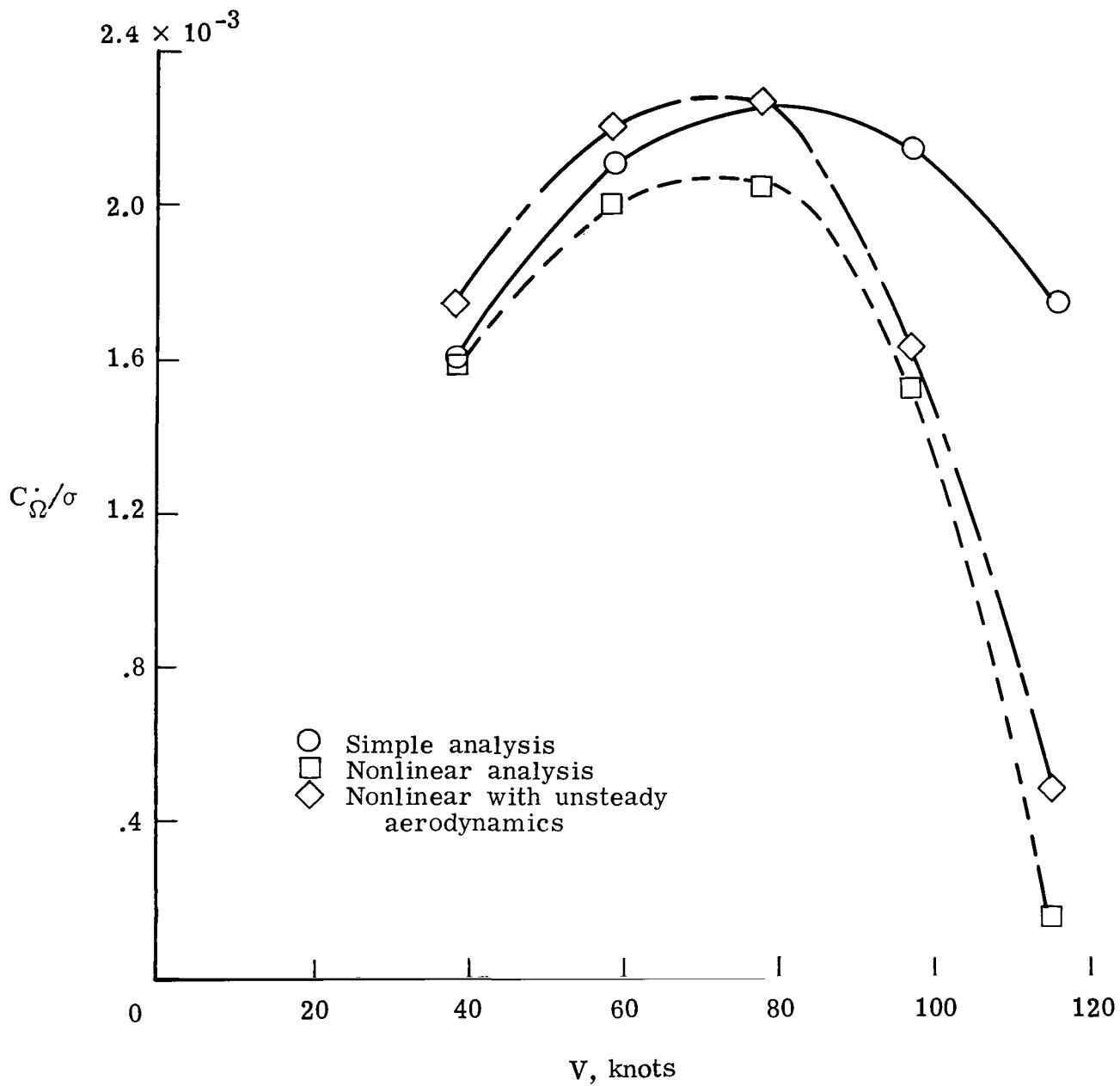


Figure 4.- Comparison of simple analysis with nonlinear analysis.
 $C_{L,R}/\sigma = 0.08$; $f/\pi R^2 = 0.01$; $\Omega R = 198.12$ m/sec.

1. Report No. NASA TP-1213 AVRADCOM TR 78-24		2. Government Accession No.		3. Recipient's Catalog No.	
4. Title and Subtitle AN ANALYSIS OF THE GUST-INDUCED OVERSPEED TRENDS OF HELICOPTER ROTORS		5. Report Date July 1978		6. Performing Organization Code	
7. Author(s) Julian L. Jenkins, Jr. and William T. Yeager, Jr.		8. Performing Organization Report No. L-12159		10. Work Unit No. 505-10-23-07	
9. Performing Organization Name and Address NASA Langley Research Center and Structures Laboratory AVRADCOM Research and Technology Laboratories Hampton, VA 23665		11. Contract or Grant No.		13. Type of Report and Period Covered Technical Paper	
12. Sponsoring Agency Name and Address National Aeronautics and Space Administration Washington, DC 20546 and U.S. Army Aviation Research and Development Command St. Louis, MO 63166		14. Army Project No. 1L262209AH76			
15. Supplementary Notes Julian L. Jenkins, Jr.: Langley Research Center. William T. Yeager, Jr.: Structures Laboratory, AVRADCOM Research and Technology Laboratories.					
16. Abstract Equations for analyzing the potential gust-induced overspeed tendency of helicopter rotors are presented and discussed. A parametric analysis has also been carried out to illustrate the sensitivity of rotor angular acceleration to changes in rotor lift, propulsive force, tip speed, and forward velocity. (This technology outlines a method for analyzing the potential gust-induced overspeed tendency of helicopter rotors.)					
17. Key Words (Suggested by Author(s)) Helicopter Gusts Rotor overspeed Flight dynamics			18. Distribution Statement Unclassified - Unlimited Subject Category 02		
19. Security Classif. (of this report) Unclassified	20. Security Classif. (of this page) Unclassified	21. No. of Pages 20	22. Price* \$4.00		

National Aeronautics and
Space Administration

SPECIAL FOURTH CLASS MAIL
BOOK

Postage and Fees Paid
National Aeronautics and
Space Administration
NASA-451



Washington, D.C.
20546

Official Business
Penalty for Private Use, \$300

3 1 10, A, 070778 S00903DS
DEPT OF THE AIR FORCE
AF WEAPONS LABORATORY
ATTN: TECHNICAL LIBRARY (SUL)
KIRTLAND AFB NM 87117

NASA

POSTMASTER: If Undeliverable (Section 158
Postal Manual) Do Not Return
